


TDP2 negatively regulates axon regeneration by inducing SUMOylation of an Ets transcription factor

Yoshiki Sakai[†], Hiroshi Hanafusa[†], Strahil Iv Pastuhov, Tatsuhiro Shimizu, Chun Li, Naoki Hisamoto^{*} & Kunihiro Matsumoto^{**} 

Abstract

In *Caenorhabditis elegans*, the JNK MAP kinase (MAPK) pathway is important for axon regeneration. The JNK pathway is activated by a signaling cascade consisting of the growth factor SVH-1 and its receptor tyrosine kinase SVH-2. Expression of the *svh-2* gene is induced by axonal injury in a process involving the transcription factors ETS-4 and CEBP-1. Here, we find that *svh-14/mlx-1*, a gene encoding a Max-like transcription factor, is required for activation of *svh-2* expression in response to axonal injury. We show that MLX-1 binds to and inhibits the function of TDPT-1, a *C. elegans* homolog of mammalian tyrosyl-DNA phosphodiesterase 2 [TDP2; also called Ets1-associated protein II (EAPII)]. Deletion of *tdpt-1* suppresses the *mlx-1* defect, but not the *ets-4* defect, in axon regeneration. TDPT-1 induces SUMOylation of ETS-4, which inhibits ETS-4 transcriptional activity, and MLX-1 counteracts this effect. Thus, TDPT-1 interacts with two different transcription factors in axon regeneration.

Keywords axon regeneration; *C. elegans*; Ets; SUMOylation; TDP2/EAPII

Subject Categories Neuroscience; Post-translational Modifications & Proteolysis

DOI 10.15252/embr.201847517 | Received 3 December 2018 | Revised 3 July 2019 | Accepted 15 July 2019 | Published online 8 August 2019

EMBO Reports (2019) 20: e47517

Introduction

A fundamental and conserved property of neurons is their ability to regenerate their axons following injury. Axon regeneration following injury is governed by an interaction between the local extracellular environment and the neuron's intrinsic growth capacity. Upon axon severance, regeneration signals are transported in a retrograde manner from the sites of damage to the nucleus, where several transcription factors are upregulated that increase the synthesis of proteins participating in neurite outgrowth [1]. Since manipulation

of these processes can improve the chances for successful axon regeneration, these signaling processes are potential targets for regeneration therapies. However, our understanding of these intrinsic signaling pathways is incomplete at present.

The nematode *Caenorhabditis elegans* is a useful model for investigating the mechanisms of axon regeneration following injury [2]. Genetic studies in *C. elegans* have identified a large number of pathways specifically involved in adult axon regeneration [3]. The *C. elegans* JNK MAP kinase (MAPK) pathway, consisting of MLK-1 (MAPKKK)–MEK-1 (MAPKK)–KGB-1 (MAPK), plays a critical role in the initiation of axon regeneration [4]. The JNK pathway is inactivated at the KGB-1 activation step by VHP-1, a member of the MAPK phosphatase family [5]. The *vhp-1* null mutation causes hyper-activation of the JNK pathway, resulting in the larval arrest of animals [5]. We recently identified new components functioning in JNK-mediated signaling by employing a genome-wide RNAi screen for suppressors of *vhp-1* lethality (*svh* genes) [6]. The *svh-1* gene encodes a growth factor-like protein homologous to mammalian HGF, and the *svh-2* gene encodes a homolog of mammalian Met, a receptor for HGF [6]. SVH-2 is a receptor tyrosine kinase (RTK) that activates the JNK pathway via tyrosine phosphorylation of the MAPKKK MLK-1. The *svh-2* gene is normally not expressed in motor neurons, but is induced in damaged motor neurons following axotomy [6]. This axotomy-induced expression of *svh-2* is regulated by ETS-4 and CEBP-1, an Ets-like transcription factor and a *C. elegans* homolog of the CCAAT/enhancer-binding protein (C/EBP), respectively [7]. Therefore, the *ets-4* mutation is defective in axon injury-induced *svh-2* expression and axon regeneration. When an axon is damaged, intracellular cAMP levels increase and cAMP-dependent protein kinase (PKA) is activated. This in turn phosphorylates ETS-4, causing the formation of a complex between ETS-4 and CEBP-1, which then activates *svh-2* transcription (Fig 1A) [7].

In the present study, we investigated the role of the *svh-14/mlx-1* gene in axon regeneration. The *mlx-1* gene encodes a Max-like transcription factor, and we have discovered that it also acts as an activator of *svh-2* expression in response to axon injury

Division of Biological Science, Graduate School of Science, Nagoya University, Nagoya, Japan

^{*}Corresponding author. Tel: +81 527 893000; E-mail: i45556a@cc.nagoya-u.ac.jp

^{**}Corresponding author. Tel: +81 527 892589; E-mail: g44177a@nucc.cc.nagoya-u.ac.jp

[†]These authors contributed equally to this work

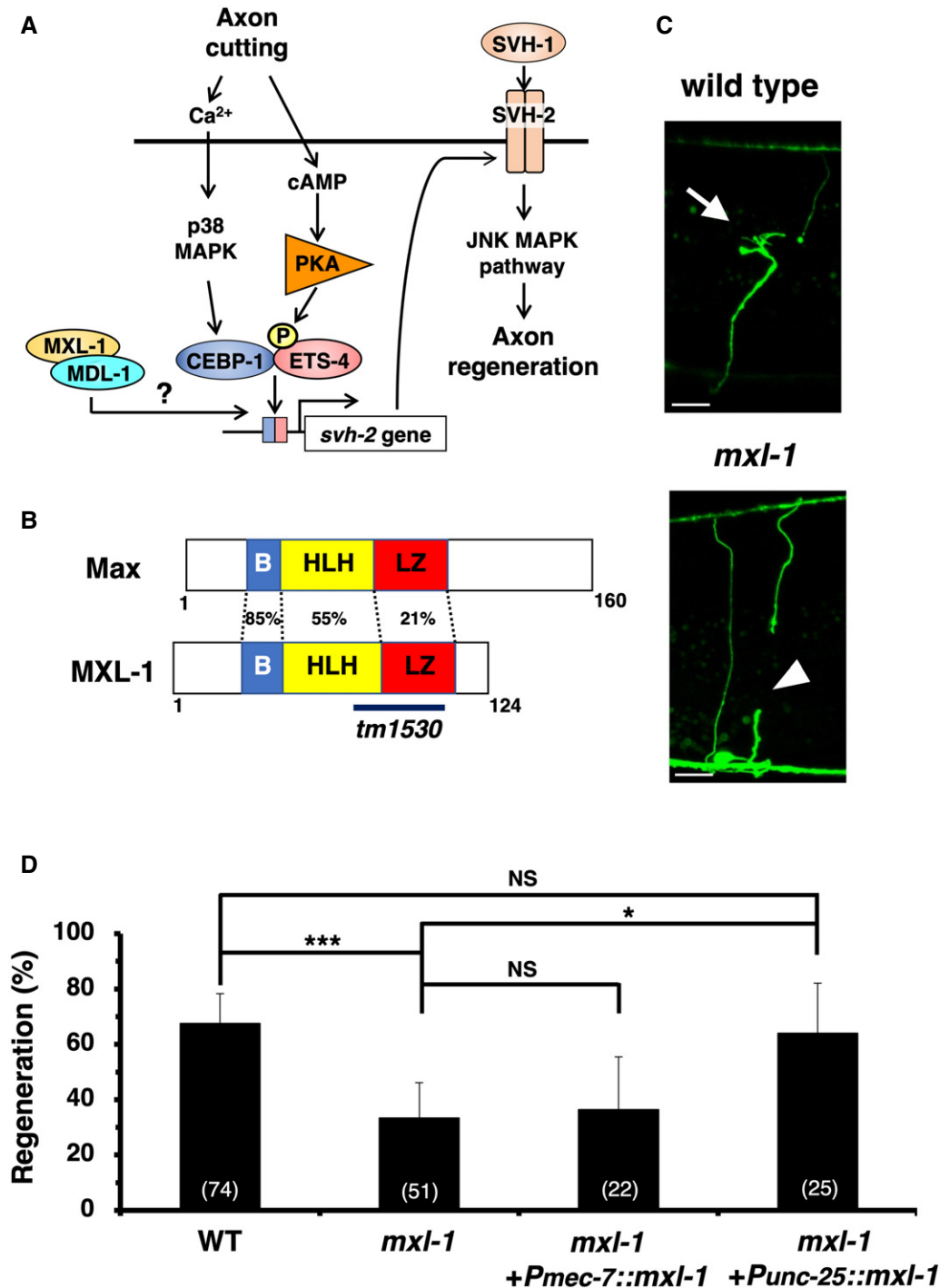


Figure 1. Identification of MXL-1 and its involvement in axon regeneration.

A Regulation of *svh-2* expression in response to axon injury. Axon injury initiates cAMP signaling and the Ca^{2+} -p38 MAPK pathway, which together function to induce the formation of an ETS-4-CEBP-1 transcription factor complex. This complex binds to the *svh-2* promoter to induce *svh-2* expression. MXL-1 forms a complex with MDL-1.

B Structure of MXL-1. Schematic diagrams of MXL-1 and its mammalian counterpart Max are shown. The domains (B-HLH-LZ) shown are the basic region (B; blue), helix-loop-helix (HLH; yellow), and leucine zipper (LZ; red). The bold line underneath indicates the extent of the deleted region in the *tm1530* deletion mutant.

C Representative D-type motor neurons in wild-type and *mxl-1* mutant animals 24 h after laser surgery. In wild-type animals, a severed axon has regenerated a growth cone (arrow). In mutants, proximal ends of axons failed to regenerate (arrowhead). Scale bar = 10 μm .

D Percentages of axons that initiated regeneration 24 h after laser surgery. The numbers (n) of animals examined are shown. Error bars indicate 95% confidence intervals (CI).

Data information: In (D), statistical significance was determined by Fisher's exact test; * $P < 0.05$; *** $P < 0.001$; NS, not significant.

and, accordingly, that the *mxl-1* mutation is defective in axon regeneration. Furthermore, we isolated TDPT-1, a homolog of mammalian TDP2 (also called EAPII), as an MXL-1-binding protein. We show that TDPT-1 inhibits the transcriptional activity of ETS-4 by inducing its SUMOylation. Thus, TDPT-1 acts as a negative regulator of axon injury-induced *svh-2* expression. These results suggest that TDPT-1 interacts with two different transcription factors and modulates their transcriptional functions in axon regeneration.

Results

SVH-14/MXL-1 is required for axon regeneration

We have previously performed a genome-wide RNAi screen for suppressors of *vhp-1* lethality and isolated 92 *svh* RNAi clones that regulate the JNK signaling pathway [6,8]. In order to find new transcription factors involved in axon regeneration, we searched among the *svh* RNAi clones for genes encoding transcription factors. In this study, we investigated the *svh-14* gene, which encodes MXL-1 [9], a *C. elegans* homolog of the mammalian Max transcription factor (Fig 1A and B). Max belongs to a member of the basic region–helix–loop–helix–leucine zipper (B-HLH-LZ) protein family [10]. *Caenorhabditis elegans* MXL-1 exhibits similarity to human Max within its B-HLH domain (Fig 1B).

To examine the effect of *mxl-1* on axon regeneration, we assayed the regrowth of laser-severed axons in γ -aminobutyric acid (GABA)-releasing D-type motor neurons (Fig 1C) [4]. In wild-type animals at the young adult stage, the regeneration of axons severed by laser was initiated within 24 h (Fig 1C and D, and Appendix Table S1). However, in *mxl-1(tm1530)* deletion mutants (Fig 1B), the frequency of axon regeneration was reduced (Fig 1C and D, and Appendix Table S1). The *mxl-1(tm1530)* mutation has no obvious effect on nerve development (Appendix Fig S1); therefore, the effect of *mxl-1* is injury-specific. To test whether MXL-1 can act in a cell-autonomous manner, we expressed *mxl-1* from the *unc-25* or *mec-7* promoter in *mxl-1(tm1530)* mutants. The *mxl-1* defect in axon regeneration was rescued by expression of *mxl-1* in D-type motor neurons by the *unc-25* promoter but not by expression in sensory neurons by the *mec-7* promoter (Fig 1D and Appendix Table S1). Furthermore, expression of *mxl-1* in D neurons of *mxl-1(tm1530)* mutants rescued regeneration to wild-type levels (Fig 1D and Appendix Table S1). These results demonstrate that MXL-1 acts to promote regeneration in a cell-autonomous manner in the damaged neuron.

MXL-1 is involved in axotomy-induced *svh-2* expression in injured neurons

Since MXL-1 is a transcription factor [9] and expression of *svh-2* is induced by axonal injury [6], we examined the genetic interaction between *mxl-1* and *svh-2*. When we generated *mxl-1(tm1530); svh-2(tm737)* double mutants, we found that the regeneration defect of the double mutant was no greater than that of the *mxl-1* single mutant (Fig 2A and Appendix Table S1), suggesting that MXL-1 and SVH-2 act in the same pathway. Furthermore, we found that constitutive expression of *svh-2* from the *Punc-25::svh-2* transgene was

able to rescue the axon regeneration defect of *mxl-1(tm1530)* mutants (Fig 2A and Appendix Table S1). This indicates that MXL-1 acts upstream of SVH-2 in the axon regeneration pathway. These results support the possibility that MXL-1 is involved in the induction of *svh-2* expression in response to axon injury.

Next, we examined whether MXL-1 regulates axon injury-induced expression of *svh-2* using a reporter construct consisting of the *svh-2* promoter, a nuclear localization signal (NLS), and the fluorescent protein VENUS (*Psvh-2::nls::venus*) [6]. In wild-type animals, axon injury induced expression of *Psvh-2::nls::venus* in D-type motor neurons (Figs 2B and EV1), as reported previously [6,7]; however, in *mxl-1(tm1530)* mutants, no induction was observed (Figs 2B and EV1). These results suggest that MXL-1 is required for axotomy-induced *svh-2* expression.

MXL-1 promotes axon regeneration by inhibiting TDPT-1 function

In mammalian systems, the transcriptional regulatory function of Max depends on its heterodimerization partner, Myc or Mad [11]. *Caenorhabditis elegans* does not have an obvious Myc ortholog but does contain a Mad-like protein MDL-1. Indeed, it has been shown that MDL-1 physically associates with the MXL-1 protein (Fig 1A) [9,12] and that the MDL-1–MXL-1 complex acts as a heterodimeric transcription factor in the regulation of aging and proteostasis [13]. Therefore, we investigated whether MDL-1 might also be involved in axon regeneration. However, we found this was not the case: In contrast to the *mxl-1* mutation, the *mdl-1(tm311)* null mutation had no effect on axon regeneration (Fig 3A and Appendix Table S1).

To understand how MXL-1 regulates *svh-2* expression in response to axon injury, we searched for additional MXL-1-binding proteins using a yeast two-hybrid screen. From this screen, we isolated three genes, *tdpt-1*, *ubc-9*, and *mdl-1* (Figs 3B and EV2). The *tdpt-1* gene encodes a homolog of mammalian TDP2 (tyrosyl-DNA phosphodiesterase 2; Fig 3C) [14]. To ask whether TDPT-1 is involved in axon regeneration, we used the CRISPR/Cas9 system to generate the mutant *tdpt-1(km68)*, which encodes a frameshift and generates a premature stop of the *tdpt-1* ORF (Fig 3C). To our surprise, we found that axon regeneration was significantly improved in *tdpt-1(km68)* mutants compared to wild-type animals (Fig 3A and Appendix Table S1). This result implies that in contrast to MXL-1, TDPT-1 negatively regulates axon regeneration. To confirm this possibility, we overexpressed TDPT-1 in D-type motor neurons of wild-type animals using the *unc-25* promoter, and indeed found that axon regeneration was decreased (Fig 3D and Appendix Table S1). These results further suggest that TDPT-1 inhibits axon regeneration cell-autonomously.

Since TDPT-1 interacts with MXL-1 but has the opposite effect on axonal regeneration, we next examined the genetic interaction between *mxl-1* and *tdpt-1*. We found that the *tdpt-1(km68)* mutation strongly suppressed the regeneration defect in *mxl-1(tm1530)* mutants (Fig 3A and Appendix Table S1). Furthermore, expression of *Psvh-2::nls::venus* in D-type neurons was induced by laser surgery in *mxl-1(tm1530); tdpt-1(km68)* double mutants (Figs 2B and EV1). However, expression of *Psvh-2::nls::venus* in D neurons of *tdpt-1(km68)* single mutants was still inducible but not constitutive (Figs 2B and EV1). These results suggest that TDPT-1 acts downstream of MXL-1 to inhibit axon regeneration through repression of

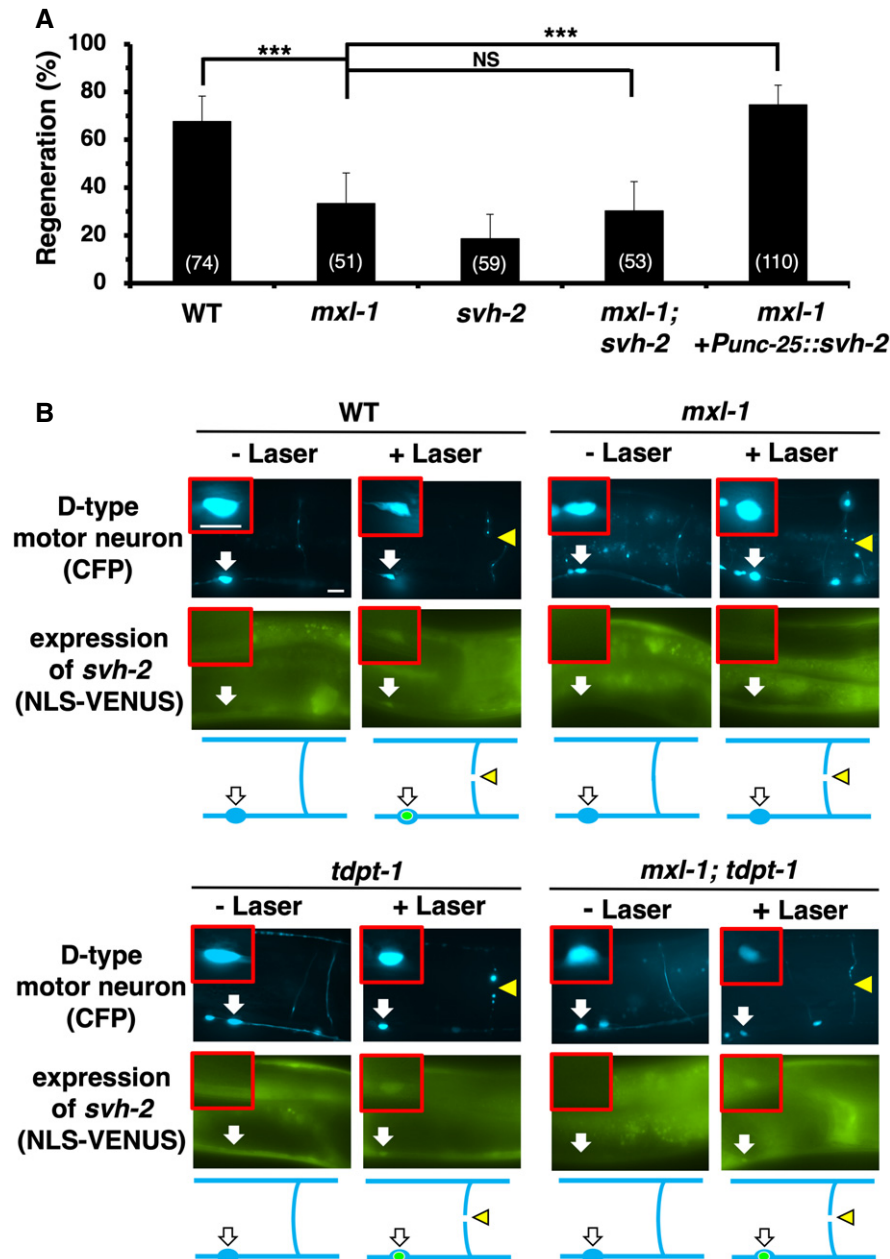


Figure 2. MXL-1 is required for the transcriptional induction of the *svh-2* gene in response to axon injury.

A Percentages of axons that initiated regeneration 24 h after laser surgery. The numbers (*n*) of animals examined are shown. Error bars indicate 95% CI.

B Induction of *Psvh-2::nls:venus* expression in D-type motor neurons by laser surgery. Expression of fluorescent proteins in D-type motor neurons of wild-type, *mxl-1*, *tdpt-1*, and *mxl-1; tdpt-1* animals 3 h after laser surgery is shown. Yellow arrowheads and white arrows indicate axon and cell bodies, respectively, of D-type neurons. White arrows indicate the sites of laser surgery. D neurons are visualized by CFP under control of the *unc-25* promoter. Cell bodies of D-type neurons are magnified and shown within the red boxes. Most of the intestinal fluorescence in these photos is from endogenous and variable background autofluorescence. A schematic representation of D-type motor neurons is shown on the bottom. Scale bars = 10 μ m.

Data information: In (A), statistical significance was determined by Fisher's exact test; ****P* < 0.001; NS, not significant.

svh-2 expression in injured neurons. This raises the possibility that MXL-1 negatively regulates TDPT-1 activity, thereby maintaining the regenerative capacity of injured neurons.

Since MXL-1 associates with both MDL-1 and TDPT-1 (Figs 3B and EV2), we asked whether these interactions compete with each other. We found that co-expression of TDPT-1 decreased the

interaction between MXL-1 and MDL-1 (Fig EV2). These results suggest that TDPT-1 and MDL-1 compete for binding to MXL-1. Consistent with this, *mdl-1* could inhibit axon regeneration when overexpressed from the *unc-25* promoter in wild-type animals, but not when overexpressed in *tdpt-1(km68)* mutants (Fig 3D and Appendix Table S1). Furthermore, in contrast to *tdpt-1*, the *mdl-1*

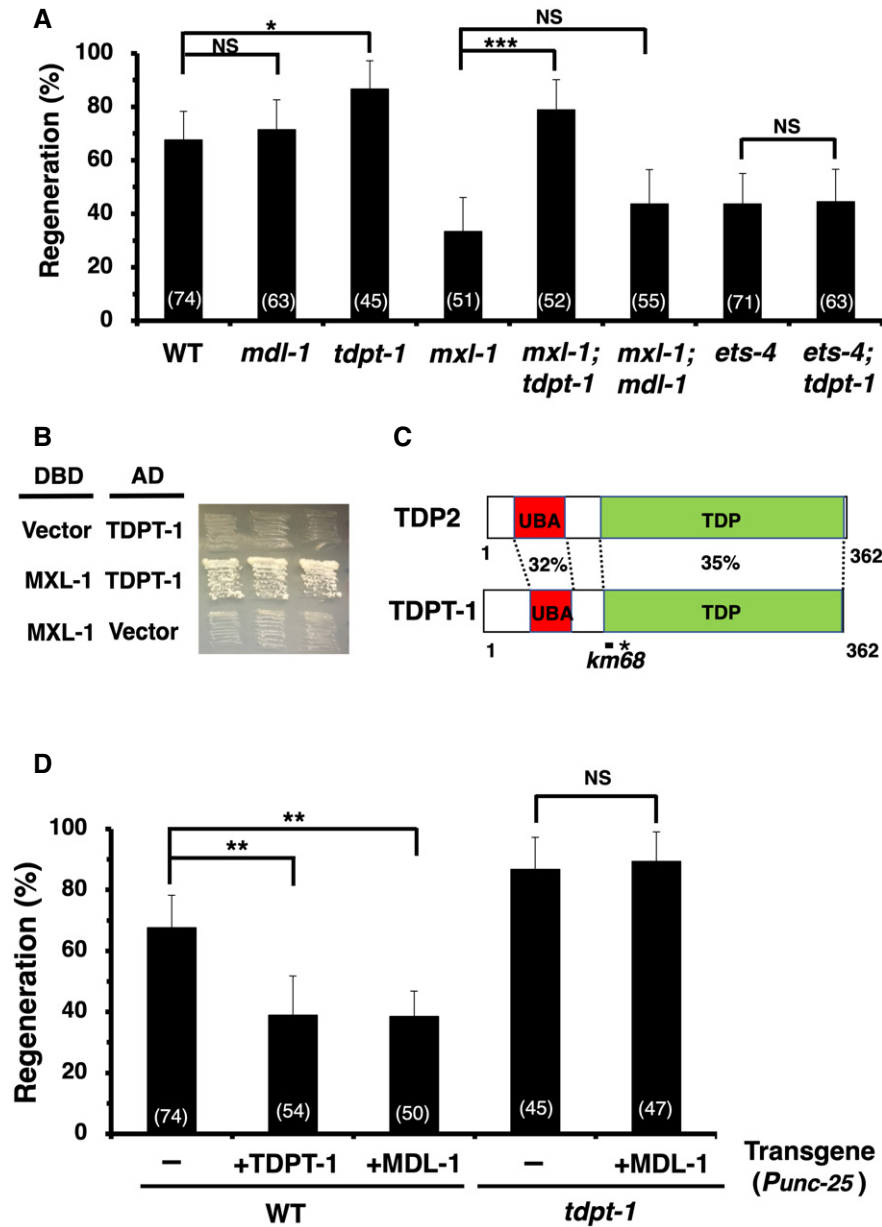


Figure 3. TDPT-1 negatively regulates axon regeneration.

A Percentages of axons that initiated regeneration 24 h after laser surgery. The numbers (*n*) of animals examined are shown. Error bars indicate 95% CI.

B Interaction of MXL-1 with TDPT-1 by yeast two-hybrid assays. The reporter yeast strain L40u was co-transformed with expression vectors encoding LexA DBD-MXL-1 and GAL4 AD-TDPT-1 as indicated. Yeasts carrying the indicated plasmids were grown on a selective plate lacking histidine and containing 10 mM 5-aminotriazole for 4 days.

C Structure of TDPT-1. Schematic diagrams of TDPT-1 and human TDP2 are shown. The domains shown are the UBA (red) and tyrosyl-DNA phosphodiesterase (TDP; green) domains. The bold line underneath indicates the extent of the deleted region (8 bp) in the *km68* mutation. An asterisk indicates a premature stop codon in *tdpt-1* caused by the *km68* deletion.

D Percentages of axons that initiated regeneration 24 h after laser surgery. The numbers (*n*) of animals examined are shown. Error bars indicate 95% CI.

Data information: In (A and D), statistical significance was determined by Fisher's exact test; **P* < 0.05; ***P* < 0.01; ****P* < 0.001; NS, not significant.

(*tm311*) mutation did not suppress the *mxl-1(tm1530)* defect in axon regeneration (Fig 3A and Appendix Table S1). These results can be explained by assuming that overexpression of MDL-1 and its interaction with MXL-1 induces the dissociation of TDPT-1 from MXL-1, resulting in an increase free TDPT-1, which in turn inhibits axon

regeneration. Thus, it is likely that overexpression of MDL-1 inhibits axon regeneration independent of its transcriptional activity.

To examine whether MDL-1 is physiologically relevant for axon regeneration, we investigated the expression pattern of *mdl-1* using a reporter consisting of *Pmdl-1::nls::gfp*. Consistent with the

cell-autonomous function of MDL-1 in the inhibition of axon regeneration, we found that the *mdl-1* gene is expressed in D-type motor neurons, and its expression was not affected by axon injury (Fig EV3A and B). We next examined the effect of axon injury on MDL-1 protein levels in D neurons using the *Punc-25::mdl-1::gfp* gene. We observed that MDL-1::GFP was localized in D neuron cell bodies (Fig EV3C). Following laser ablation of the axons, MDL-1::GFP expression decreased in D neurons (Fig EV3C and D). Taken together, these results suggest that axon injury induces degradation of MDL-1 resulting in the formation of free MXL-1, which associates with TDPT-1 and inhibits its negative effect on axon regeneration.

TDPT-1 induces SUMOylation of ETS-4

How does TDPT-1 negatively regulate axon regeneration? We have previously demonstrated that the ETS-4–CEBP-1 complex activates *svh-2* expression in response to axon injury (Fig 4A) [7]. Mammalian TDP2 was also independently identified as EAPII (Ets1-associated protein II) because of its association with the Ets1 transcription factor and was shown to modulate the transcriptional activity of Ets1 [15]. Since *C. elegans* ETS-4 belongs to the Ets transcription factor family [16], we examined the relationship between TDPT-1 and ETS-4. In contrast to MXL-1, we found that the *tdpt-1(km68)* mutation was unable to suppress the regeneration defect caused by the *ets-4(ok165)* mutation (Fig 3A and Appendix Table S1), suggesting that ETS-4 functions downstream of TDPT-1 in the axon regeneration pathway. These findings are consistent with a model in which TDPT-1 modulates ETS-4 activity, similar to the mammalian EAPII/TDP2, and thereby inhibits axon regeneration.

Next, we examined whether TDPT-1 can physically interact with ETS-4 by co-immunoprecipitation in mammalian COS-7 cells. T7-tagged TDPT-1 was co-expressed with HA-tagged ETS-4 in COS-7 cells, immunoprecipitated with anti-T7 antibody, and HA-ETS-4 probed by immunoblotting with anti-HA antibody. We found that ETS-4 indeed co-immunoprecipitated with TDPT-1 (Fig 4B). Since ETS-4 is phosphorylated by PKA at Ser-73 [7], we investigated whether PKA phosphorylation of ETS-4 Ser-73 would affect its interaction with TDPT-1. We found that the phosphorylation-negative mutant ETS-4(S73A) and a phosphorylation-mimicked form of ETS-4, ETS-4(S73E), associated with TDPT-1 to a similar extent as wild-type ETS-4 (Fig 4B). These results suggest that ETS-4 interacts with TDPT-1 and that the phosphorylation state of ETS-4 has no effect on this interaction.

Mammalian TDP2 interacts with SUMO-2, a ubiquitin-like modifier; UBC9, a SUMO E2 conjugating enzyme; and ZNF451, a SUMO E3/E4 ligase [17,18]. Therefore, we examined whether TDPT-1 affects SUMOylation of ETS-4. We first tested whether ETS-4 is SUMOylated *in vitro*. We expressed HA-ETS-4 from mammalian COS-7 cells and then incubated the immunopurified HA-ETS-4 with human SUMO-2, E1, UBC9, and ATP. We found that HA-ETS-4 was efficiently SUMOylated *in vitro* (Fig 4C). To identify the SUMOylated residue, we analyzed the ETS-4 protein sequence for potential SUMOylation sites. SUMOylation occurs on a lysine residue within the consensus motif ϕ -Lys-Xxx-Glu (ϕ ; large hydrophobic residue) [19]. We found that ETS-4 contains two consensus SUMOylation motifs: Val-Lys(32)-Ser-Glu and Val-Lys(83)-Asn-Glu (Fig 4D). Consistent with this, a mutant version of ETS-4 in which both lysine residues were replaced with alanines, ETS-4(K32A; K83A), showed no SUMOylation (Fig 4C).

We next examined whether TDPT-1 enhances SUMOylation of ETS-4. When T7-TDPT-1 was added in SUMOylation assay by its co-expression with HA-ETS-4 in COS-7 cells, we observed little enhancement of ETS-4 SUMOylation *in vitro* by TDPT-1 (Fig EV4). We therefore investigated the effect of TDPT-1 on ETS-4 SUMOylation *in vivo* of mammalian cells. To test whether ETS-4 is SUMOylated in mammalian cells, we co-expressed HA-ETS-4 and His-tagged SUMO-1 or SUMO-2 with or without T7-TDPT-1 in HEK293 cells. SUMO-modified proteins were purified from cell lysates by cobalt affinity chromatography, and SUMO-ETS-4 conjugates were analyzed by immunoblotting with anti-HA antibody. When ETS-4, SUMO-2, and TDPT-1 were co-expressed, SUMO-modified ETS-4 proteins were detected (Fig 4E). No bands were observed in the absence of TDPT-1 co-expression. In addition, when His-SUMO-1 was co-expressed, we did not detect SUMOylation of ETS-4 (Fig 4E). When HA-ETS-4(K32A; K83A) was co-expressed with His-SUMO-2 and T7-TDPT-1, no SUMOylation was observed (Fig 4E). These results indicate that TDPT-1 expression induces SUMOylation of ETS-4 at Lys-32 and Lys-83 in mammalian cells. Furthermore, we found that co-expression of MXL-1-Myc inhibited TDPT-1-induced SUMOylation of HA-ETS-4 (Fig 4E). The fact that enhancement of ETS-4 SUMOylation by TDPT-1 was detected in mammalian cells but not *in vitro* suggests that TDPT-1 expression induces SUMOylation of ETS-4 by inhibiting its de-SUMOylation.

Next we examined the interplay between the phosphorylation and SUMOylation of ETS-4. We co-expressed T7-TDPT-1 and His-SUMO-2 with HA-ETS-4(S73A) or HA-ETS-4(S73E) in HEK293 cells. We found that both ETS-4(S73A) and ETS-4(S73E) were SUMOylated, although SUMOylation of ETS-4(S73E) was slightly decreased (Fig 5A). Thus, the phosphorylation state of ETS-4 S73 has little effect on SUMOylation. This is also consistent with the observation that phosphorylation of ETS-4 S73 had no effect on the interaction between ETS-4 and TDPT-1 (Fig 4B). Next, we tested the effect of ETS-4 SUMOylation on Ser-73 phosphorylation. HA-ETS-4 was expressed in COS-7 cells, and we performed *in vitro* kinase assays with active PKA and immunopurified HA-ETS-4. We confirmed that PKA could phosphorylate HA-ETS-4 but not HA-ETS-4(S73A) (Fig 5B). Thus, PKA phosphorylates the Ser-73 residue of ETS-4 *in vitro*. However, when we took immunopurified HA-ETS-4, subjected this to *in vitro* SUMOylation and then incubated it with active PKA, the non-SUMOylated form of HA-ETS-4 was phosphorylated but the SUMOylated form was not (Fig 5B). These results suggest that SUMOylation of ETS-4 inhibits its PKA-mediated Ser-73 phosphorylation.

The effect of SUMOylation on ETS-4 function in axon regeneration

If SUMOylation is important for the inhibition of ETS-4 function, then mutations defective in SUMOylation might affect axon regeneration. UBC-9 is an E2 SUMO conjugating enzyme that catalyzes the formation of an isopeptide bond between the C-terminal glycine of SUMO and lysine [20]. *Caenorhabditis elegans* contains the single gene *smo-1* encoding SUMO. We found that similar to the *tdpt-1* mutation, *ubc-9(tm2610)* and *smo-1(ok359)* mutations caused a significant improvement in axon regeneration compared to animals carrying the wild-type genes (Fig 6A and Appendix Table S1). Overexpression of *ets-4* did not enhance axon regeneration in *ubc-9*

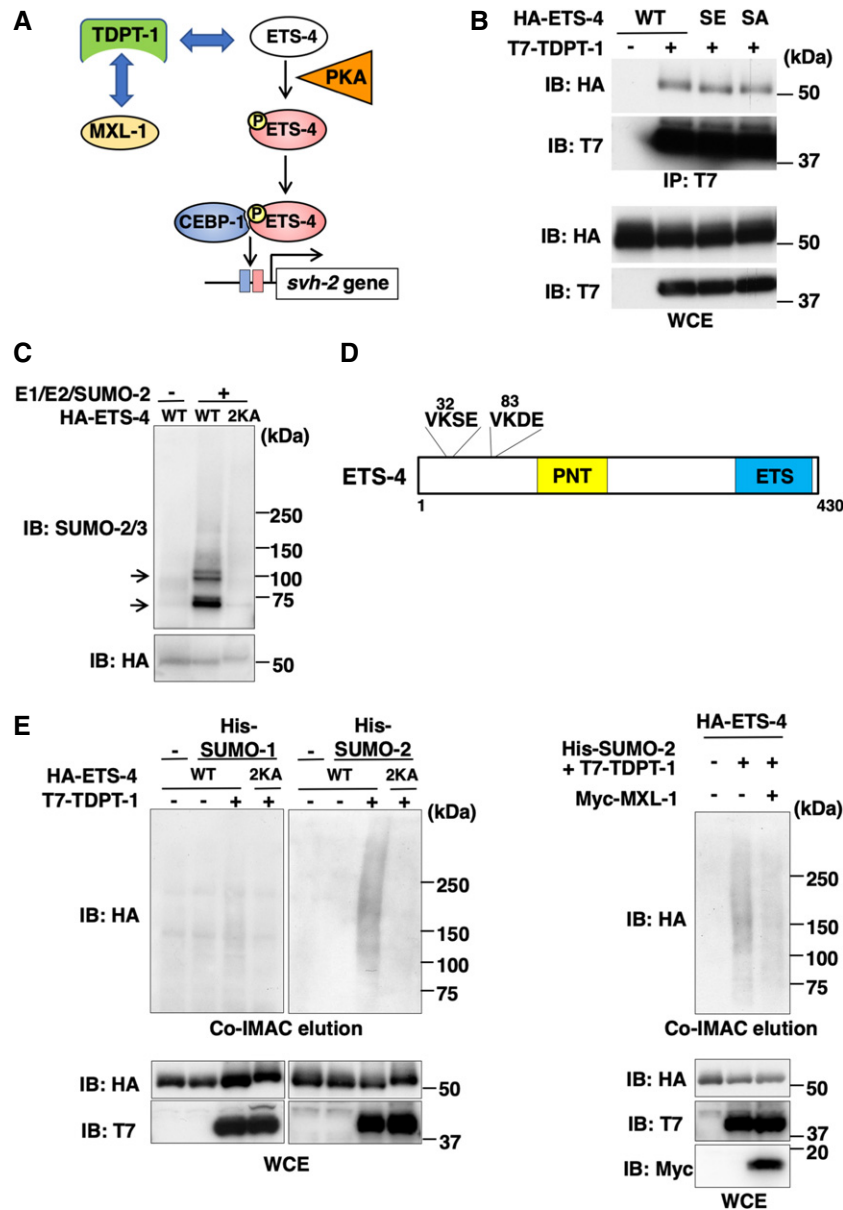


Figure 4. TDPT-1 induces SUMOylation of ETS-4.

A Relationship among MXL-1, TDPT-1, ETS-4, CEBP-1, and PKA in the regulation of axon injury-induced *svh-2* expression.

B Interaction between ETS-4 and TDPT-1. COS-7 cells were transfected with plasmids encoding T7-TDPT-1, HA-ETS-4 (WT), HA-ETS-4(S73E) (SE), and HA-ETS-4(S73A) (SA), as indicated. Whole-cell extracts (WCE) and immunoprecipitated complexes obtained with anti-T7 antibody (IP: T7) were analyzed by immunoblotting (IB).

C In vitro SUMOylation of ETS-4. COS-7 cells were transfected with plasmids encoding HA-ETS-4 (WT) and HA-ETS-4(K32A; K83A) (2KA), as indicated. Cell lysates were immunoprecipitated with anti-HA antibody. The immunoprecipitates were subjected to *in vitro* SUMOylation assays. Reaction mixtures were analyzed by immunoblotting (IB) with anti-SUMO-2/3 and anti-HA antibodies. Arrows mark the SUMOylated-ETS-4 bands.

D Schematic representation of the two putative consensus SUMOylation sites and domain structure in ETS-4. Domains are shown as follows: a pointed domain (PNT; yellow) and an Ets DNA-binding domain (ETS; blue).

E SUMOylation of ETS-4 in mammalian cells. HEK293 cells were transfected with plasmids encoding HA-ETS-4 (WT), HA-ETS-4(K32A; K83A) (2KA), T7-TDPT-1, His-SUMO-1, His-SUMO-2, and MXL-1-Myc, as indicated. SUMO-conjugated proteins were isolated by cobalt affinity chromatography. ETS-4 was detected by immunoblotting with anti-HA antibody. Whole-cell extracts (WCE) were analyzed by immunoblotting (IB).

(*tm2610*) mutants (Fig 6A and Appendix Table S1). We next examined the genetic interaction between *ubc-9* and *tdpt-1*. We found that overexpression of *tdpt-1* was unable to inhibit axon regeneration in *ubc-9(tm2610)* mutants (Fig 6A and Appendix Table S1). Thus, the

inhibitory effect of *tdpt-1* overexpression on axon regeneration is dependent on SUMOylation. These results suggest that TDPT-1 functions upstream of UBC-9-mediated SUMOylation or inhibits de-SUMOylation of ETS-4. Furthermore, we found that *ubc-9(tm2610)*

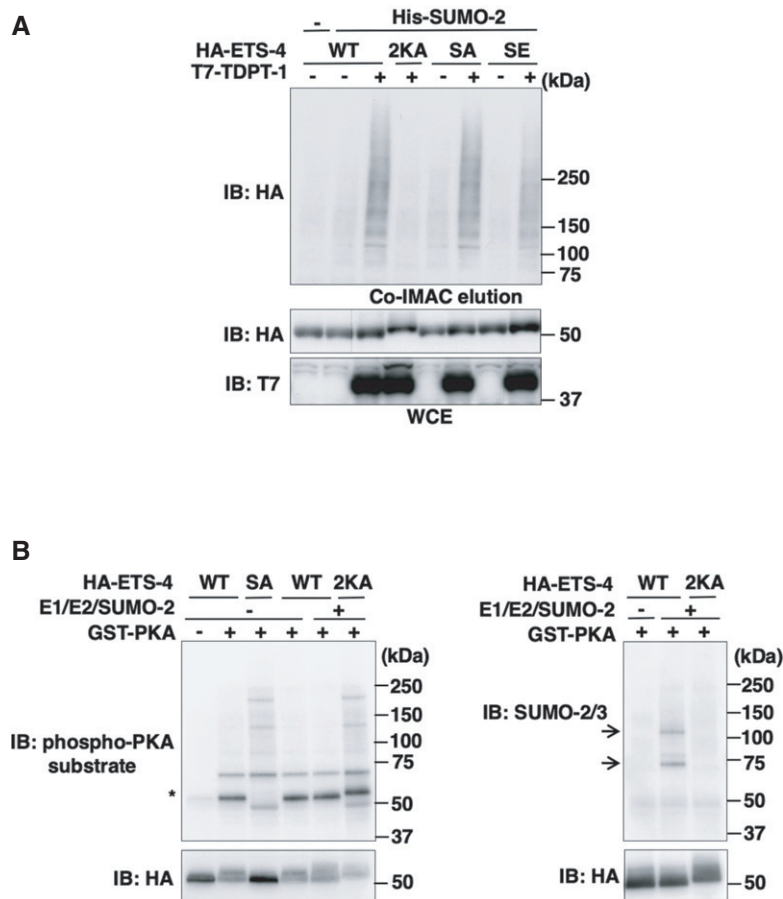


Figure 5. The interplay between the phosphorylation and SUMOylation of ETS-4.

A Effect of phosphorylation of ETS-4 on SUMOylation of ETS-4 in mammalian cells. HEK293 cells were transfected with plasmids encoding HA-ETS-4 (WT), HA-ETS-4 (K32A; K83A) (2KA), HA-ETS-4(S73A) (SA), HA-ETS-4(S73E) (SE), T7-TDPT-1, and His-SUMO-2, as indicated. SUMO-conjugated proteins were isolated by cobalt affinity chromatography. ETS-4 was detected by immunoblotting with anti-HA antibody. Whole-cell extracts (WCE) were analyzed by immunoblotting (IB).

B Effect of SUMOylation of ETS-4 on PKA phosphorylation of ETS-4 *in vitro*. COS-7 cells were transfected with plasmids encoding HA-ETS-4 (WT), HA-ETS-4(S73A) (SA), and HA-ETS-4(K32A; K83A) (2KA), as indicated. Cell lysates were immunoprecipitated with anti-HA antibody. The immunoprecipitates were subjected to *in vitro* PKA kinase assays or *in vitro* SUMOylation and then *in vitro* PKA kinase assays, using recombinant GST-fused active PKA, as indicated. Reaction mixtures were analyzed by immunoblotting (IB) with anti-phospho-PKA substrate, anti-SUMO-2/3, and anti-HA antibodies. Arrows mark the SUMOylated-ETS-4 bands. Asterisk indicates the non-SUMOylated- and phosphorylated-ETS-4 bands.

and *smo-1(ok359)* mutations suppressed the axon regeneration defect observed in *mxl-1(tm1530)* mutants (Fig 6B and Appendix Table S1). In addition, the *ets-4(K32A; K83A)* mutation also suppressed the *mxl-1(tm1530)* defect (Fig 6C and Appendix Table S1). These results support a model in which SUMOylation of ETS-4 is necessary for the inhibition of axon regeneration and MXL-1 counters this by reducing TDPT-1-mediated SUMOylation of ETS-4.

Phosphorylation of ETS-4 at Ser-73 by PKA is required for complex formation with CEBP-1, which activates transcription of the *svh-2* gene (Fig 4A) [7]. If SUMOylation of ETS-4 inhibits its phosphorylation at Ser-73, and phosphorylation at Ser-73 promotes axon regeneration, then the phospho-mimetic *ets-4(S73E)* mutation should suppress the *mxl-1* defect in axon regeneration. This would be similar to what was observed with the *ets-4(K32A; K83A)* mutation, which is defective in ETS-4 SUMOylation. As expected, we found that *ets-4(S73E)* ameliorated the observed defect in axon regeneration in *mxl-1(tm1530)* mutants (Fig 6C and

Appendix Table S1). In contrast, the *ets-4(K32A; K83A; S73A)* triple mutation, which is defective in both SUMOylation and phosphorylation, is unable to suppress the *mxl-1(tm1530)* defect in axon regeneration (Fig 6C and Appendix Table S1). Thus, disruption of ETS-4 SUMOylation does not bypass the requirement for phosphorylation at Ser-73 in axon regeneration. These results suggest that ETS-4 SUMOylation inhibits phosphorylation of ETS-4 Ser-73, resulting in the inhibition of its transcriptional activity. Although the *ets-4(K32A; K83A)* and *ets-4(S73E)* mutations were able to suppress the *mxl-1(tm1530)* defect in axon regeneration (Fig 6C and Appendix Table S1), this suppression was not as strong as seen with the *tdpt-1(km68)*, *ubc-9(tm2610)*, or *smo-1(ok359)* mutations (Figs 3A and 6B, and Appendix Table S1). Furthermore, expression of *ets-4(K32A; K83A)* or *ets-4(S73E)* in wild-type animals did not increase the frequency of axon regeneration (Appendix Fig S2 and Table S1). These results suggest that TDPT-1 may inhibit axon regeneration by inducing SUMOylation of another factor in addition to ETS-4.

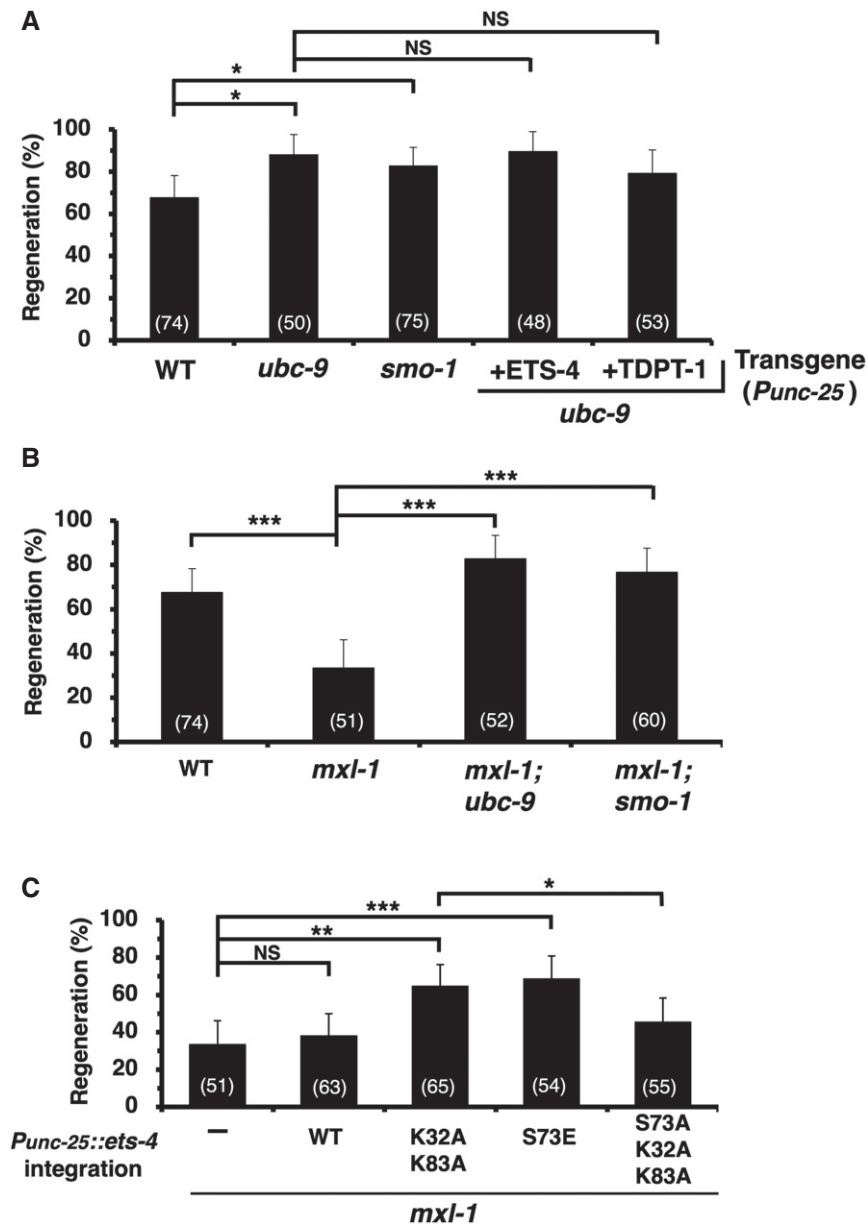


Figure 6. Effects of SUMOylation of ETS-4 on axon regeneration.

A–C Percentages of axons that initiated regeneration 24 h after laser surgery are shown. The numbers (*n*) of animals examined are shown. Error bars indicate 95% CI.

Data information: In (A–C), statistical significance was determined by Fisher's exact test; **P* < 0.05; ***P* < 0.01; ****P* < 0.001; NS, not significant.

Discussion

In *C. elegans*, axon regeneration is activated by the SVH-1 growth factor, its receptor SVH-2, and the JNK signaling pathway [6]. The *svh-2* gene is not expressed in D-type motor neurons under normal conditions, but is induced in response to neuronal damage [6]. This upregulation appears to critically involve the physical interaction of the Ets-like factor ETS-4 and the C/EBP-like factor CEBP-1, which in concert activate the *svh-2* promoter [7]. Axon injury activates PKA, which phosphorylates ETS-4, thereby promoting its association with CEBP-1. This ETS-4–CEBP-1 complex binds to the promoter region

of *svh-2* and activates its transcription. In this study, we identified Max-like MXL-1 as another transcription factor involved in axon injury-induced expression of *svh-2*. In mammals, Max regulates transcription of gene expression as part of a complex with Mad [11]. Similarly, *C. elegans* MXL-1 associates with the Mad-like MDL-1 [9,12]. These two proteins need to form heterodimers in order to bind DNA, suggesting that each protein requires the other to effect its function. Indeed, the MDL-1–MXL-1 complex has been shown to have a role in longevity and proteostasis [13]. However, in contrast to the *mxl-1* mutation, the *mdl-1* loss-of-function mutation has no effect on axon regeneration. Furthermore, MXL-1 cannot form a

homodimer and by itself is unable to bind to DNA [9]. These results suggest that MXL-1 may not regulate transcription of the *svh-2* gene by directly binding to the promoter region.

How does MXL-1 regulate expression of *svh-2* in response to axon injury? This regulation seems to involve TDPT-1, which we isolated as an MXL-1-binding protein. The *tdpt-1* deletion mutation is able to suppress the *mxl-1* defect but not the *ets-4* defect in axon regeneration, indicating that TDPT-1 acts between MXL-1 and ETS-4 to negatively regulate axon regeneration. TDPT-1 is homologous to mammalian TDP2, which was also independently identified as EAPII, a protein that binds to the Ets1 transcription factor [15]. EAPII inhibits the transcriptional activity of Ets1. Similarly, *C. elegans* TDPT-1 also associates with ETS-4 and inhibits its ability to transactivate *svh-2* expression. These results suggest that MXL-1 activates *svh-2* transcription in response to axon injury by interacting with TDPT-1 and relieving its inhibition of ETS-4 activity.

How does TDPT-1 inhibit ETS-4 transcriptional activity? Mammalian TDP2 is the first in a series of enzymes that removes adducts at the 5'-phosphotyrosyl bond of DNA complexed with topoisomerases (TOPs) [14]. Recently, it was shown that TDP2 is involved in the SUMOylation of TOP2 [18]. Consistent with this, we found that TDPT-1 also induces SUMO modification of ETS-4 when expressed in mammalian cells. Since TDP2 associates with SUMO-modified TOP2 and stabilizes its SUMOylated state, it is likely that TDPT-1 association with ETS-4 inhibits its de-SUMOylation. The transcriptional activity of mammalian Ets1 is also negatively regulated by SUMOylation [21]. Furthermore, negative regulation by SUMOylation was also observed for the *C. elegans* factor LIN-1, a member of the Ets transcription factor family [22,23]. Although SUMOylation promotes transcriptional repression in mammals and *C. elegans*, the molecular mechanism by which this occurs has not been well defined [24]. Here, we show that SUMO modification of ETS-4 negatively affects its transcription-activating function. We observed that mutation of the SUMOylation sites in ETS-4 or inhibition of the SUMOylation process by the *smo-1* and *ubc-9* mutations suppresses the *mxl-1* defect in axon regeneration. These results argue for an important role of SUMO modification in ETS-4 transcriptional activity. This transcriptional activity requires the formation of a complex between ETS-4 and CEBP-1, which is promoted by phosphorylation of ETS-4 by PKA [7]. We show that SUMOylation of ETS-4 inhibits PKA phosphorylation of ETS-4. Furthermore, an *ets-4* mutation that mimics the phosphorylated state also suppresses the *mxl-1* defect in axon regeneration. These biochemical and genetic data raise the possibility that SUMO modification of ETS-4 interferes with PKA-mediated phosphorylation, thereby inhibiting formation of the ETS-4-CEBP-1 complex and preventing the transcriptional activation of *svh-2*. Taken together, our analyses indicate that TDPT-1 is a negative modulator of ETS-4 activity that probably functions by inhibiting ETS-4 interaction with its co-activator CEBP-1. Importantly, we found that aspects of these regulatory relationships are evolutionarily conserved: (i) Both TDP2 and TDPT-1 inhibit the transcriptional activity of Ets family transcription factors; (ii) TDP2 and TDPT-1 both modulate SUMOylation; and (iii) SUMOylation inactivates the activities of the Ets family transcription factors. TDP2 and TDPT-1 may represent novel components in signal transduction that regulate eukaryotic gene expression in response to extracellular signals.

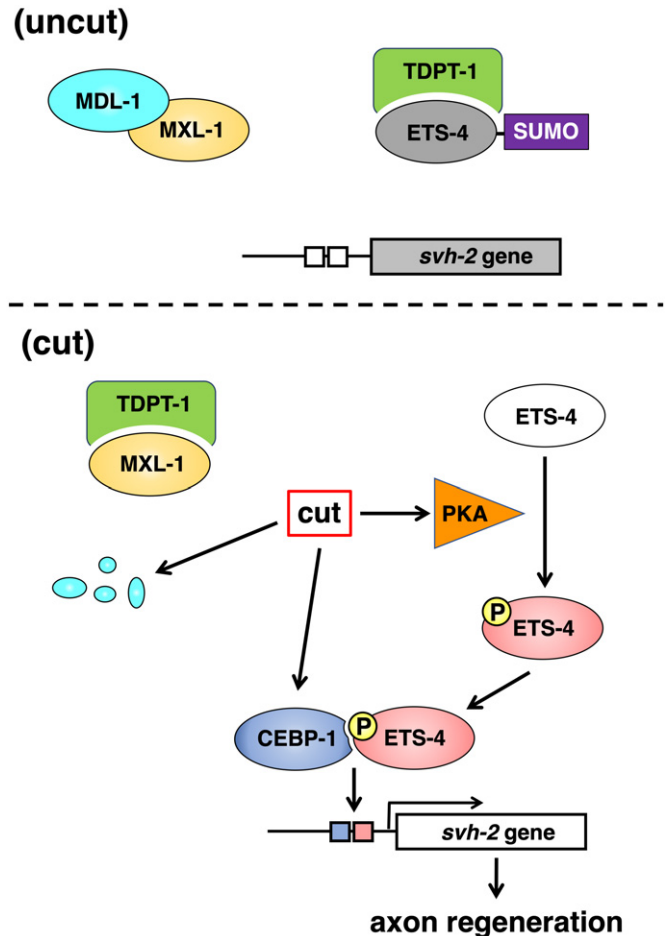


Figure 7. Schematic diagram for the regulation of ETS-4 by TDPT-1 in axon regeneration.

In this study, we show that MXL-1 stimulates the transcriptional activity of ETS-4 by inhibiting TDPT-1-mediated SUMOylation. Based on our findings, we propose the following molecular mechanism by which MXL-1 regulates axonal regeneration in D-type motor neurons after nerve injury (Fig 7). Under normal conditions, MXL-1 forms a complex with MDL-1, and TDPT-1 interacts with ETS-4 to induce its SUMOylation, resulting in the repression of ETS-4 transcriptional activity. Axon injury leads to the degradation of MDL-1, and free MXL-1 can now interact with TDPT-1. Next, ETS-4 is released from TDPT-1 and is de-SUMOylated, allowing PKA to phosphorylate ETS-4 and subsequently activate signaling. These findings thus expand our understanding of the functions of MXL-1 and TDPT-1 as key regulators of axon regeneration.

Materials and Methods

C. elegans strains

The *C. elegans* strains used in this study are listed in Appendix Table S2. All strains were maintained on nematode

growth medium (NGM) plates and fed with bacteria of the OP50 strain by the standard method [25].

Plasmids

Punc-25::mxl-1, *Punc-25::tdpt-1*, and *Punc-25::mdl-1* were generated by inserting each cDNA isolated from a cDNA library into the pSC325 vector. *Pmec-7::mxl-1* was generated by inserting the *mxl-1* cDNA into the pPD52.102 vector. *Punc-25::mdl-1::gfp* was constructed by inserting a GFP fragment into the *Punc-25::mdl-1* plasmid by a standard Gibson assembly reaction using NEBuilder HiFi DNA Assembly Master Mix (NEB). *Punc-25::svh-2*, *Punc-25::ets-4*, *Punc-25::ets-4(S73A)*, and *Punc-25::ets-4(S73E)* plasmids have been described previously [6,7]. *Punc-25::ets-4(K32A; K83A)* and *Punc-25::ets-4(S73A; K32A; K83A)* were made by oligonucleotide-directed PCR using *Punc-25::ets-4* and *Punc-25::ets-4(S73A)* as templates, respectively, and the mutations were verified by DNA sequencing. To make *Pmdl-1::nls::gfp*, a 5 kbp DNA fragment just upstream of the start codon of the *mdl-1* gene was amplified from wild-type genomic DNA by PCR and inserted into the pPD95.70 vector. *Punc-25::cfp* and *Psvh-2::nls::venus* plasmids have been described previously [7]. The T7-TDPT-1, His-SUMO-1, and His-SUMO-2 plasmids were generated by inserting the *tdpt-1*, SUMO-1, and SUMO-2 cDNAs into the pCMV-T7 and pcDNA3.1/His B vectors, respectively. The HA-ETS-4, HA-ETS-4(S73A), and HA-ETS-4(S73E) plasmids have been described previously [7]. The HA-ETS-4(K32A; K83A) was made by oligonucleotide-directed PCR using HA-ETS-4 as a template, and the mutations were verified by DNA sequencing. The MXL-1-Myc construct was made by inserting the *mxl-1* cDNA into the pCMV-Myc-C vector (Clontech). The LexA DBD-MXL-1 plasmid was made by inserting the *mxl-1* cDNA into the pBTM116 vector. The GAL4 AD-TDPT-1 and GAL4 AD-MDL-1 plasmids were made by inserting the *tdpt-1* and *mdl-1* cDNAs into the pACTII vector, respectively [26]. The pKT10-TDPT-1 plasmid was made by inserting the *tdpt-1* cDNA into the pKT10 vector [27].

Generation of the *tdpt-1* mutation using CRISPR–Cas9

The *tdpt-1(km68)* deletion mutant was generated using the CRISPR–Cas9 system [28]. The *pU6::tdpt-1_sgRNA* was made by replacing the *unc-119* target sequence of *pU6::unc-119_sgRNA* (Addgene) with 5'-CGGGAGTGAGGCGTTCGAG-3', corresponding to the genomic sequence within the *tdpt-1* gene. The *pU6::tdpt-1_sgRNA* (50 ng/μl) was co-injected together with the *Peft-3::cas9-sv40_nls::tbb-2* 3'UTR (30 ng/μl) and *Pmyo-2::dsred-monomer* (25 ng/μl) plasmids into KU501 strain. An F1 animal carrying the transgene was picked, and genomic DNA from its descendants was subjected to a heteroduplex mobility assay [29] to detect the presence of short insertions or deletions in the *tdpt-1* gene. The descendants of these animals were selected to obtain the *tdpt-1* homozygous mutant. The *tdpt-1(km68)* mutation is an 8-bp deletion in the *tdpt-1* gene, causing a frameshift and premature stop codon in exon 3.

Transgenic animals

Transgenic animals were obtained by the standard *C. elegans* microinjection method [30]. *Pmyo-2::dsred-monomer* (25 ng/μl), *Punc-25::mxl-1* (50 ng/μl), *Pmec-7::mxl-1* (50 ng/μl), *Punc-25::tdpt-1* (50 ng/μl), *Punc-25::mdl-1* (50 ng/μl), *Punc-25::ets-4* (50 ng/μl),

Punc-25::ets-4(K32A; K83A) (50 ng/μl), *Punc-25::ets-4(S73E)* (50 ng/μl), *Punc-25::cfp* (50 ng/μl), *Psvh-2::nls::venus* (75 ng/μl), *Pmdl-1::nls::gfp* (25 ng/μl), and *Punc-25::mdl-1::gfp* (25 ng/μl) plasmids were used in *kmEx1512* [*Punc-25::mxl-1* + *Pmyo-2::dsred-monomer*], *kmEx1513* [*Pmec-7::mxl-1* + *Pmyo-2::dsred-monomer*], *kmEx1515* [*Punc-25::tdpt-1* + *Pmyo-2::dsred-monomer*], *kmEx1517* [*Punc-25::mdl-1* + *Pmyo-2::dsred-monomer*], *kmEx1519* [*Punc-25::ets-4* + *Pmyo-2::dsred-monomer*], *kmEx1521* [*Punc-25::ets-4(K32A; K83A)* + *Pmyo-2::dsred-monomer*], *kmEx1522* [*Punc-25::ets-4(S73E)* + *Pmyo-2::dsred-monomer*], *kmEx1527* [*Punc-25::cfp* + *Psvh-2::nls::venus* + *Pmyo-2::dsred-monomer*], *kmEx1531* [*Pmdl-1::nls::gfp* + *Pmyo-2::dsred-monomer*], and *kmEx1532* [*Punc-25::mdl-1::gfp* + *Pmyo-2::dsred-monomer*], respectively. The *kmIs1523* [*Punc-25::ets-4* + *NeoR*], *kmIs1524* [*Punc-25::ets-4(K32A; K83A)* + *NeoR*], *kmIs1525* [*Punc-25::ets-4(S73E)* + *NeoR*], and *kmIs1526* [*Punc-25::ets-4(S73A; K32A; K83A)* + *NeoR*] integrated transgenes were made by the miniMos technique [31], using a *NeoR* plasmid carrying the *unc-25* promoter driving each *ets-4* cDNA and the *unc-54* 3'UTR. The *kmEx501* extrachromosomal and *wplIs36* integrated arrays have been previously described [6,32].

Microscopy

Standard fluorescent images of transgenic animals were observed under an ×100 objective of a Nikon ECLIPSE E800 fluorescent microscope and photographed with a Zyla CCD camera. Confocal fluorescent images were taken on Olympus FV-500 or Zeiss LSM-800 confocal laser-scanning microscopes with an ×63 objective.

Axotomy

Axotomy and microscopy were performed as described previously [6]. In brief, the hermaphrodite animals at the young adult stage were randomly selected and subjected to axotomy. Imaged commissures that had growth cones or small branches present on the proximal fragment were counted as “regenerated”. Proximal fragments that showed no change after 24 h were counted as “no regeneration”. A minimum of individuals with 1–3 axotomized commissures were observed for most experiments.

Quantification of VENUS expression

Expression of VENUS fluorescence was quantified using the ImageJ program (NIH). The cell bodies of severed D neurons were identified by the relative position of D neurons [33]. They were outlined with closed polygons, and the fluorescent intensities within these areas were determined (I_s). As controls, the cell bodies of unsevered D neurons in the same animal were analyzed similarly (I_u). To determine the background intensity of each cell, the same polygon was placed in the area neighboring the cell body and fluorescence was measured (I_{bs} and I_{bu} , respectively). The relative signal intensity (I_r) normalized by unsevered D neuron was calculated as $(I_s - I_{bs}) / (I_u - I_{bu})$. Cells having an $I_r > 5$ were categorized as “expressed”.

Data acquisition and quantification of MDL-1::GFP after axotomy

Z-stack fluorescent images of animals expressing mCherry and MDL-1::GFP in their D-type motor neurons were obtained by

confocal microscopy (Zeiss LSM-800). Images were taken every 15 min for 5 h starting shortly after axotomy of some of the MDL-1::GFP-expressing neurons. The stability of MDL-1::GFP after axotomy was assayed by calculating the relative intensity of MDL-1 in the following way. First, an elliptical region of interest (ROI) roughly corresponding to the cell nucleus was determined for each cell expressing MDL-1::GFP, and the mean fluorescent intensities of GFP and mCherry were measured for this ROI to obtain $I_{MDL-1::GFP}$ and $I_{mCherry}$, respectively. Next, the background was estimated by measuring the mean GFP (or mCherry) intensity of an adjacent region of the same size ($I_{MDL-1::GFP(BG)}$, $I_{mCherry(BG)}$). The ratio of background-subtracted MDL-1::GFP to mCherry intensity was calculated for two time points – immediately after axotomy: $I_{MDL-1::GFP}/I_{mCherry}(0) = (I_{MDL-1::GFP} - I_{GFP(BG)}) / (I_{mCherry} - I_{mCherry(BG)})$ and 5 h after axotomy: $I_{MDL-1::GFP}/I_{mCherry}(5) = (I_{MDL-1::GFP} - I_{GFP(BG)}) / (I_{mCherry} - I_{mCherry(BG)})$. Finally, the relative intensity of MDL-1::GFP, $RI_{MDL-1::GFP}(5)$ at 5 h after axotomy was calculated as: $RI_{MDL-1::GFP}(5) = I_{MDL-1::GFP}/I_{mCherry}(5) / I_{MDL-1::GFP}/I_{mCherry}(0)$. $RI_{MDL-1::GFP}(5)$ values were calculated both for neurons with intact ($n = 13$) and severed axons ($n = 16$), and data were plotted using the R functions `boxplot` and `stripchart` in RStudio [35].

Yeast two-hybrid screening and analysis

Yeast two-hybrid screening using the LexA DBD-MXL-1 plasmid was performed as described previously [34]. For yeast two-hybrid analysis, GAL4 AD-TDPT-1 and pACTII plasmids were co-transformed with either LexA DBD-MXL-1 or the pBTM116 vector into the *Saccharomyces cerevisiae* reporter strain L40u [*MATa trp1 ura3 leu2 his3 LYS2::(lexAop)₄HIS3*] and allowed to grow on SC-Leu-Trp plates. Transformants grown on these plates were then streaked out onto SC-Leu-Trp-His plates with 10 mM 5-aminotriazole (AT) and incubated at 30°C for 4 days. The pKT10-TDPT-1 or pKT10 vector was further transformed into yeast carrying LexA DBD-MXL-1 and GAL4 AD-MDL-1. The transformants were selected on SC-Leu-Trp-Ura plates, streaked onto SC-Leu-Trp-Ura-His (–His) or SC-Leu-Trp-Ura (+His) plates with 10 mM AT, and incubated at 30°C for 4 days.

Immunoprecipitation

For immunoprecipitation, transfected COS-7 cells were lysed in RIPA buffer [50 mM Tris-HCl, pH 7.4, 0.15 M NaCl, 0.25% deoxycholic acid, 1% NP-40, 1 mM EDTA, 1 mM dithiothreitol, 1 mM phenylmethylsulfonyl fluoride, phosphatase inhibitor cocktail 2 and 3 (Sigma), and protease inhibitor cocktail (Sigma)], followed by centrifugation at $15,000 \times g$ for 12 min. The supernatant was added to 10 μ l (bed volume) of Dynabeads Protein G (Invitrogen) with anti-T7 antibody (PM022; MBL) and rotated for 2 h at 4°C. The beads were then washed three times with ice-cold phosphate-buffered saline (PBS) and subjected to immunoblotting.

Immunoblotting

After cell extracts were subjected to SDS-PAGE, proteins were transferred to a polyvinylidene difluoride membrane (Hybond-P; GE Healthcare). The membranes were immunoblotted with anti-HA antibody (mouse 16B12; BioLegend) or anti-T7 antibody (mouse T7-Tag; Merck; or rabbit PM022; MBL), and bound antibodies were

visualized with horseradish peroxidase (HRP)-conjugated antibodies against rabbit or mouse IgG using an HRP chemiluminescent substrate reagent kit (Novex ECL; Invitrogen).

In vitro SUMOylation assays

In vitro SUMOylation of ETS-4 was carried out using the SUMOylation assay kit (Abcam) according to the manufacturer's instructions. Briefly, immunopurified HA-ETS-4 or HA-ETS-4(K32A; K83A) from transfected COS-7 cells was suspended in reaction buffer (20 μ l) containing SUMO activating enzyme (E1), UBC9 (E2), SUMO-2, and ATP. Following 1 h of incubation at 37°C, reactions were terminated using Laemmli sample buffer and boiling. SUMOylated ETS-4 was detected by immunoblotting with mouse anti-SUMO-2/3 antibody (ab139470; Abcam).

In vitro kinase assays

ETS-4 proteins were immunopurified from transfected COS-7 cells. SUMOylated ETS-4 was prepared from the *in vitro* SUMOylation assay described above. Kinase reactions were performed in a final volume of 20 μ l buffer consisting of 25 mM MOPS (pH 7.2), 12.5 mM glycerol phosphate, 25 mM MgCl₂, 2 mM EDTA, 0.25 mM DTT, 200 μ M ATP, and 0.4 μ g of recombinant PKA (Carna Biosciences). Samples were incubated for 20 min at 30°C and the reactions terminated by addition of Laemmli sample buffer and boiling. Phosphorylation of ETS-4 was detected by immunoblotting with rabbit anti-phospho-PKA substrate antibody (100G7E; Cell Signaling).

Cobalt affinity pull-down assay

His-SUMO-2-ETS-4 conjugates were purified by cobalt-based immobilized metal affinity chromatography (Co-IMAC). Transfected human HEK293 cells (mycoplasma-free) were lysed in denaturing buffer containing 8 M urea, 20 mM imidazole, and 0.1% Triton X-100 in phosphate-buffered saline (PBS), followed by sonication and centrifugation at $15,000 \times g$ for 5 min. The supernatant was added to 10 μ l (bed volume) of Dynabeads His-Tag Isolation & Pull-down beads (Invitrogen) and rotated for 1 h at 4°C. The beads were then washed three times with ice-cold denaturing buffer and one time with ice-cold PBS, followed by elution in 30 μ l sample buffer (AE-1430 EzApply; ATTO) supplemented with 300 mM imidazole.

Statistical analysis

Statistical analyses were carried out as described previously [6]. Briefly, confidence intervals (95%) were calculated by the modified Wald method and two-tailed *P*-values were calculated using Fisher's exact test (<http://www.graphpad.com/quickcalcs/contingency1/>). The Welch *t*-test and the Wilcoxon rank sum test (two-tailed) were performed by using a *t*-test calculator (<http://www.graphpad.com/quickcalcs/ttest1/>) and the R function `wilcox.test()`, respectively.

Expanded View for this article is available online.

Acknowledgements

We thank Dr. Asako Sugimoto (Tohoku Univ.), *Caenorhabditis* Genetic Center (CGC), National Bio-Resource Project, and *C. elegans* Knockout

Consortium for materials. Some strains were provided by the CGC, which is funded by NIH Office of Research Infrastructure Programs (P40 OD10440). This work was supported by grants from the Ministry of Education, Culture and Science of Japan (to H.H., S.P., N.H., and K.M.) and the Project for Elucidating and Controlling Mechanisms of Aging and Longevity from Japan Agency for Medical Research and Development, AMED, under Grant Number JP19gm5010001 (to N.H.).

Author contributions

YS, HH, NH, and KM designed the experiments, analyzed the data, and wrote the manuscript. YS, HH, SIP, TS, CL, and NH performed experiments.

Conflict of interest

The authors declare that they have no conflict of interest.

References

- Moore DL, Goldberg JL (2011) Multiple transcription factor families regulate axon outgrowth and regeneration. *Dev Neurobiol* 71: 1186–1211
- Yanik MF, Cinar H, Cinar HN, Chisholm AD, Jin Y, Ben-Yakar A (2004) Neurosurgery: functional regeneration after laser axotomy. *Nature* 432: 822
- Hammarlund M, Jin Y (2014) Axon regeneration in *C. elegans*. *Curr Opin Neurobiol* 27: 199–207
- Nix P, Hisamoto N, Matsumoto K, Bastiani MJ (2011) Axon regeneration requires co-activation of p38 and JNK MAPK pathways. *Proc Natl Acad Sci USA* 108: 10738–10743
- Mizuno T, Hisamoto N, Terada T, Kondo T, Adachi M, Nishida E, Kim DH, Ausubel FM, Matsumoto K (2004) The *Caenorhabditis elegans* MAPK phosphatase VHP-1 mediates a novel JNK-like signaling pathway in stress response. *EMBO J* 23: 2226–2234
- Li C, Hisamoto N, Nix P, Kanao S, Mizuno T, Bastiani M, Matsumoto K (2012) The growth factor SVH-1 regulates axon regeneration in *C. elegans* via the JNK MAPK cascade. *Nat Neurosci* 15: 551–557
- Li C, Hisamoto N, Matsumoto K (2015) Axon regeneration is regulated by Ets-C/EBP transcription complexes generated by activation of the cAMP/Ca²⁺ signaling pathways. *PLoS Genet* 11: e1005603
- Shimizu T, Pastuhov SI, Hanafusa H, Matsumoto K, Hisamoto N (2018) The *C. elegans* BRCA2-ALP/Enigma complex regulates axon regeneration via a Rho GTPase-ROCK-MLC phosphorylation pathway. *Cell Rep* 24: 1880–1889
- Yuan J, Tirabassi RS, Bush AB, Cole MD (1998) The *C. elegans* MDL-1 and MXL-1 proteins can functionally substitute for vertebrate MAD and MAX. *Oncogene* 17: 1109–1118
- Blackwood EM, Eisenman RN (1991) Max: a helix-loop-helix zipper protein that forms a sequence-specific DNA-binding complex with Myc. *Science* 251: 1211–1217
- Amati B, Land H (1994) Myc-Max-Mad: a transcription factor network controlling cell cycle progression, differentiation and death. *Curr Opin Genet Dev* 4: 102–108
- Pickett CL, Breen KT, Ayer DE (2007) A *C. elegans* Myc-like network cooperates with semaphorin and Wnt signaling pathways to control cell migration. *Dev Biol* 310: 226–239
- Johnson DW, Llop JR, Farrell SF, Yuan J, Stolzenburg LR, Samuelson AV (2014) The *Caenorhabditis elegans* Myc-Mondo/Mad complexes integrate diverse longevity signals. *PLoS Genet* 10: e1004278
- Cortes Ledesma F, El Khamisy SF, Zuma MC, Osborn K, Caldecott KW (2009) A human 5'-tyrosyl DNA phosphodiesterase that repair topoisomerase-mediated DNA damage. *Nature* 461: 674–678
- Pei H, Yordy JS, Leng Q, Zhao Q, Watson DK, Li R (2003) EAPII interacts with ETS1 and modulates its transcriptional function. *Oncogene* 22: 2699–2709
- Thyagarajan B, Blaszczak AG, Chandler KJ, Watts JL, Johnson WE, Graves BJ (2010) ETS-4 is a transcriptional regulator of life span in *Caenorhabditis elegans*. *PLoS Genet* 6: e1001125
- Eisenhardt N, Chaugule VK, Koidl S, Droscher M, Dogan E, Rettich J, Sutinen P, Imanishi SY, Hofmann K, Palvimo JJ et al (2015) A new vertebrate SUMO enzyme family reveals insights into SUMO-chain assembly. *Nat Struct Mol Biol* 22: 959–967
- Schellenberg MJ, Lieberman JA, Herrero-Ruiz A, Butler LR, Williams JG, Muñoz-Cabello AM, Mueller GA, London RE, Cortés-Ledesma F, Williams RS (2017) ZATT (ZNF451)-mediated resolution of topoisomerase 2 DNA-protein cross-links. *Science* 357: 1412–1416
- Shampson DA, Wang M, Matunis MJ (2001) The small ubiquitin-like modifier-1 (SUMO-1) consensus sequence mediates Ubc9 binding and is essential for SUMO-1 modification. *J Biol Chem* 276: 21664–21669
- Jones D, Crowe E, Stevens TA, Candido EP (2002) Functional and phylogenetic analysis of the ubiquitination system in *Caenorhabditis elegans*: ubiquitin-conjugating enzymes, ubiquitin-activating enzymes, and ubiquitin-like proteins. *Genome Biol* 3: 2.1–2.15
- Nishida T, Terashima M, Fukami K (2006) PIASy-mediated repression of the Ets-1 is independent of its sumoylation. *Biochem Biophys Res Commun* 345: 1536–1546
- Leight ER, Glossip D, Kornfeld K (2005) Sumoylation of LIN-1 promotes transcriptional repression and inhibition of vulval cell fates. *Development* 132: 1047–1056
- Leight ER, Murphy JT, Fantz DA, Pepin D, Schneider DL, Ratliff TM, Mohammad DH, Herman MA, Kornfeld K (2015) Conversion of the LIN-1 ETS protein of *Caenorhabditis elegans* from a SUMOylated transcriptional repressor to a phosphorylated transcriptional activator. *Genetics* 199: 761–775
- Garrett-Sinha LA (2013) Review of Ets1 structure, function, and roles in immunity. *Cell Mol Life Sci* 70: 3375–3390
- Brenner S (1974) The genetics of *Caenorhabditis elegans*. *Genetics* 77: 71–94
- Li L, Elledge SJ, Peterson CA, Bales ES, Legerski RJ (1994) Specific association between the human DNA repair proteins XPA and ERCC1. *Proc Natl Acad Sci USA* 91: 5012–5016
- Tanaka K, Nakafuku M, Tamanoi F, Kajiro Y, Matsumoto K, Toh-e A (1990) IRA2, a second gene of *Saccharomyces cerevisiae* that encodes a protein with a domain homologous to mammalian ras GTPase-activating protein. *Mol Cell Biol* 10: 4303–43413
- Friedland AE, Tzur YB, Esvelt KM, Colaiácovo MP, Church GM, Calarco JA (2013) Heritable genome editing in *C. elegans* via a CRISPR-Cas9 system. *Nat Methods* 10: 741–743
- Zou S (1997) A practical approach to genetic screening for influenza virus variants. *J Clin Microbiol* 35: 2623–2627
- Mello CC, Kramer JM, Stinchcomb D, Ambros V (1991) Efficient gene transfer in *C. elegans*: extrachromosomal maintenance and integration of transforming sequences. *EMBO J* 10: 3959–3970

31. Frøkjær-Jensen C, Davis MW, Hopkins CE, Newman BJ, Thummel JM, Olesen SP, Grunnet M, Jørgensen EM (2008) Single-copy insertion of transgenes in *Caenorhabditis elegans*. *Nat Genet* 40: 1375–1383
32. Firnhaber C, Hammarlund M (2013) Neuron-specific RNAi in *C. elegans* and its use in a screen for essential genes required for GABA neuron function. *PLoS Genet* 9: e1003921
33. Hall DH, Altun ZF (2007) *C. elegans* atlas. Cold Spring Harbor, NY: Cold Spring Harbor Laboratory Press
34. Sakamoto R, Byrd DT, Brown HM, Hisamoto N, Matsumoto K, Jin Y (2005) The *Caenorhabditis elegans* UNC-14 RUN domain protein binds

to the kinesin-1 and UNC-16 complex and regulates synaptic vesicle localization. *Mol Biol Cell* 16: 483–496

35. RStudio Team (2015) *RStudio: integrated development for R*. Boston, MA: RStudio, Inc. URL <http://www.rstudio.com/>



License: This is an open access article under the terms of the Creative Commons Attribution-NonCommercial-NoDerivs 4.0 License, which permits use and distribution in any medium, provided the original work is properly cited, the use is non-commercial and no modifications or adaptations are made.